



UNIVERSITY OF LEEDS

This is a repository copy of *Understanding the Friction Reduction Mechanism Based on Molybdenum Disulfide Tribofilm Formation and Removal*.

White Rose Research Online URL for this paper:  
<http://eprints.whiterose.ac.uk/139975/>

Version: Accepted Version

---

**Article:**

Xu, D, Wang, C, Espejo, C et al. (3 more authors) (2018) Understanding the Friction Reduction Mechanism Based on Molybdenum Disulfide Tribofilm Formation and Removal. *Langmuir*, 34 (45). pp. 13523-13533. ISSN 0743-7463

<https://doi.org/10.1021/acs.langmuir.8b02329>

---

© 2018 American Chemical Society. This is an author produced version of a paper published in *Langmuir*. Uploaded in accordance with the publisher's self-archiving policy.

**Reuse**

Items deposited in White Rose Research Online are protected by copyright, with all rights reserved unless indicated otherwise. They may be downloaded and/or printed for private study, or other acts as permitted by national copyright laws. The publisher or other rights holders may allow further reproduction and re-use of the full text version. This is indicated by the licence information on the White Rose Research Online record for the item.

**Takedown**

If you consider content in White Rose Research Online to be in breach of UK law, please notify us by emailing [eprints@whiterose.ac.uk](mailto:eprints@whiterose.ac.uk) including the URL of the record and the reason for the withdrawal request.



[eprints@whiterose.ac.uk](mailto:eprints@whiterose.ac.uk)  
<https://eprints.whiterose.ac.uk/>

# Understanding the Friction Reduction Mechanism Based on the Molybdenum Disulfide Tribofilm Formation and Removal

Dichu Xu<sup>1,2,\*</sup>, Chun Wang<sup>2</sup>, Cayetano Espejo<sup>2</sup>, Jiugen Wang<sup>1</sup>, Anne Neville<sup>2</sup>, Ardian Morina<sup>2,\*</sup>

<sup>1</sup> School of Mechanical Engineering, Zhejiang University, Hangzhou, 310027, Zhejiang, China

<sup>2</sup> Institute of Functional Surfaces, School of Mechanical Engineering, University of Leeds, Leeds LS2 9JT, UK

**ABSTRACT:** Among friction modifier lubricant additives, molybdenum dialkyldithiocarbamate (MoDTC) provides excellent friction behavior in boundary lubricated tribocontacts. It is well established that the low friction obtained with MoDTC is as a result of the formation of lattice structure MoS<sub>2</sub> nanosheets. However, the relationship between the molybdenum species quantity, its distribution on the contact surface and the friction behavior is not yet fully understood. In this work, Raman microscopy and Atomic Force Microscopy (AFM) have been used with the aim of understanding the link between the friction behavior and the MoDTC/ZDDP tribofilm formation and removal. Tribotests were coupled with a collection of ex-situ Raman intensity maps to analyze the MoS<sub>2</sub> tribofilm build-up. Post-test AFM analyses were implemented on the ball wear scar to acquire the average MoDTC/ZDDP tribofilm thickness. In-situ Raman spectra analyses were carried out to detect the MoS<sub>2</sub> tribofilm removal. A good correlation was achieved between the friction coefficient measurements and Raman maps when using a linear relationship between the microscopic friction and the local amount of MoS<sub>2</sub> tribofilm. After a rapid increase, the average MoDTC/ZDDP tribofilm thickness levels out to a steady state as the friction drop ceases. The removal rate of MoS<sub>2</sub> from tribofilms, obtained at different temperatures, suggests that the MoS<sub>2</sub> tribofilms are much easier to be removed from tribocontacts compared to anti-wear ZDDP tribofilms. This is the first study that sets out a framework to link MoS<sub>2</sub> amount and coverage to the friction behavior, providing the basis for developing numerical models capable of predicting friction by taking into account tribochemistry processes.

## INTRODUCTION

It has been reported that about 11.5% of fuel energy in passenger cars is consumed due to frictional losses in automotive engines.<sup>1</sup> One of the main objectives in engine oil development is to improve fuel consumption efficiency by reducing frictional losses in tribological contacts. To achieve this target, oils with low viscosity are increasing in popularity which, however, will result in engine tribological systems being run in the boundary lubrication regime for a large part of their operational cycle. In this circumstance, not only increased friction but also excessive wear would compromise engine performance.

It is well established that the use of lubricant additives is crucial to improve the tribological performance of lubricated systems. The widely used friction modifier molybdenum dialkyldithiocarbamate (MoDTC) and the ubiquitous antiwear/antioxidant zinc dialkyldithiophosphate (ZDDP) are an excellent proof of this fact.<sup>2,3</sup> It is important to understand that there are dynamic processes which involve the tribofilm formation and removal during the tribological contact, and that the balance between formation and removal leads toward tribofilm build-up which has a direct impact on friction and wear evolution.<sup>4-6</sup> Predicting the performance of lubricant additives in engine tribology systems has become one of the most important research areas within the development of optimized energy-efficient systems.<sup>7</sup>

It has been widely accepted that the formation of molybdenum disulfide MoS<sub>2</sub> platelets,<sup>8,9</sup> as a result of MoDTC ‘tribochemical reactions’,<sup>10-13</sup> contributes to the friction reduction in the boundary lubrication regime. A

model was developed to explore the structure, dynamics and tribological properties of MoS<sub>2</sub> in an idealized system.<sup>14</sup> However, the relationship between the molybdenum species quantity, its distribution on the contact surfaces and the friction behavior is not yet established.

By means of several surface analytical techniques, studies of the MoDTC/ZDDP tribofilm composition and structure have related the MoS<sub>2</sub> forming on the surface to the friction reduction onset. X-ray Photoelectron Spectroscopy (XPS) and Energy Dispersive X-ray analysis (EDX) have commonly been used *ex-situ* in the chemical characterization of MoDTC/ZDDP tribofilms.<sup>15,16</sup> The use of a combination of XPS with high-resolution Transmission Electron Microscopy (TEM) demonstrated that the friction reduction is due to sliding between two separate MoS<sub>2</sub> single sheets.<sup>8</sup> Also, tribological tests showed that the MoDTC additive lost its friction-reducing effectiveness during rubbing time,<sup>17</sup> but no quantitative *in-situ* studies on the removal behavior of the MoS<sub>2</sub> tribofilms have been undertaken.

Raman spectroscopy, especially when combined with Atomic Force Microscopy (AFM)<sup>18</sup> and TEM,<sup>19</sup> is a very powerful technique to detect MoS<sub>2</sub> tribofilms in the wear scar. Two distinct Raman peaks (centered at 383 and 412 cm<sup>-1</sup>) are attributed to the MoS<sub>2</sub> structure. Khaemba et al.<sup>20</sup> detected FeMoO<sub>4</sub> as a product of MoDTC decomposition using Raman spectroscopy. It is difficult to differentiate FeMoO<sub>4</sub> and MoO<sub>3</sub> using XPS since they are of same oxidation state and hence have similar Mo 3d peaks. But they have distinct peaks in Raman spectra. Rai et al.<sup>19</sup> used Raman map analyses to evaluate the transient processes of the MoS<sub>2</sub> tribofilm formation. Raman spectroscopy has been demonstrated to have a great potential for the identification and measurement of the spatial distribution of molybdenum species in the tribofilm. However, it still remains to be seen whether it can be used for the *quantitative* analysis of MoS<sub>2</sub> tribofilm and distribution toward the frictional behavior, bearing in mind the patchy nature of these films.

The aim of this paper is to probe the functional relationship between friction and MoS<sub>2</sub> tribofilm quantity/distribution on the wear scar. *Ex-situ* time-resolved Raman spectroscopy mapping has been used to acquire the MoS<sub>2</sub> tribofilm amount and distribution. A discussion of two possible friction reduction models - one is based on a binary model describing the relationship between friction coefficient and the coverage ratio of the wear scar area covered by MoS<sub>2</sub>, while the other is based on a linear relationship between the microscopic friction coefficient and the local amount of MoS<sub>2</sub> tribofilm - is presented to contribute to the understanding of how MoS<sub>2</sub> growth on the contact area leads to friction reduction. The proposed models are then tested by how good the fit is between the friction coefficient measurements and the MoS<sub>2</sub> tribofilm amount as calibrated from Raman maps. Post-test AFM experiments capture the evolution of the MoDTC/ZDDP tribofilm thickness. *In-situ* Raman

spectroscopy analyses are implemented to detect and quantify the removal of MoS<sub>2</sub> tribofilms from the MoDTC/ZDDP tribofilm matrix.

## EXPERIMENTAL METHODOLOGY

**Tribological tests.** Tribotests were conducted using a ball-on-disc tribometer under boundary lubricated condition. The steel discs used in the tests had a thickness of 1 mm with an inner diameter and outer diameter of 85 mm and 110 mm respectively, whereas the ball had a diameter of 6.35 mm. The ball was fixed to a loading arm, which used a dead weight to apply a load against the rotating disc. Oil temperature was set using two heat cartridges connected to a thermal controller which used the feedback provided by two K-type thermocouples. Both the speed and the position of the rotating disc are controlled using a DC motor attached to a computer. The friction force was measured by a load cell during the experiment. The friction coefficient was calculated by the Labview software on the attached PC. Table 1 lists the tribological tests conducted in the boundary lubrication regime in this study. Tribotests were performed at 80 °C and 120 °C to form the MoS<sub>2</sub> films as a function of time. Tests were run from 2.5 to 30 minutes, which were covering the whole friction reduction period. After the tribotests, the sample discs were rinsed using heptane.

To confirm that the tribotests are run in the boundary lubrication regime, the lambda ratio was calculated using the following equation

$$\lambda = \frac{h_{\min}}{\sqrt{R_{q1}^2 + R_{q2}^2}} \quad (1)$$

where  $R_{q1}$ ,  $R_{q2}$  are the root mean square roughness of the disc and ball, and  $h_{\min}$  is the dimensionless minimum film thickness for a point contact is obtained using the Dowson and Hamrock equation<sup>21</sup>

$$h_{\min} = 3.63 \times R \times U^{0.68} \times G^{0.49} \times W^{-0.073} (1 - e^{-0.68k_e}) \quad (2)$$

with  $R$  being the effective radius of the contact,  $G$  the dimensionless material parameter,  $U$  the dimensionless speed parameter,  $W$  the dimensionless load parameter, and  $k_e$  is the ellipticity. Table 2 gives the detailed information on the lubricants and materials.

**Table 1 Tribological tests conducted in the ball-on-disc tribometer**

Tribotests	Tribofilm formation tests	Tribofilm removal tests
Max. Hertzian pressure		1.0 GPa
Sliding speed		0.25 m/s
Bulk temperature		80 °C, 120 °C
Lubricants	PAO+1%wt ZDDP+0.5%wt MoDTC	PAO+1%wt ZDDP+0.5%wt MoDTC; PAO+1%wt ZDDP
Test duration (min)	2.5, 5, 15, 30	0~20 (removal time)

**Table 2 Conditions for tribological tests in the boundary lubrication regime**

Samples	Disc: AISI 1074, ball: AISI 52100
Dimensions	Inner/outer diameter of the disc: 85 mm/110 mm Diameter of the ball: 6.35 mm
Roughness r.m.s	Disc: 200 nm, ball: 17 nm
Young's modulus	210 GPa (Disc and Ball)
Poisson ratio	0.3 (Disc and Ball)
Absolute Viscosity (mPa·s)	10.5 (80 °C)
Pressure-viscosity coefficient (GPa <sup>-1</sup> )	12.1 (80 °C) <sup>22</sup>
Lambda ratio	≤0.038

**Raman mapping of MoS<sub>2</sub> tribofilm growth.** Friction reduction from MoDTC additive is mainly due to the formation of MoS<sub>2</sub> nanosheets in the tribocontact. MoS<sub>2</sub> forms as a result of decomposition of the MoDTC additive when the tribochemical reactions are activated on rubbing surfaces, in addition to some contribution from running-in and the shakedown behavior of asperities during tribocontacts. Raman spectroscopy can easily identify MoS<sub>2</sub> formation on the MoDTC/ZDDP tribofilm surfaces by the presence of two distinct Raman peaks at 383 and 412 cm<sup>-1</sup> which are attributed to the MoS<sub>2</sub> crystalline structure, as shown in Figure 1A. In this section, Raman spectroscopy was used to monitor the intensity map and subsequent coverage growth of MoS<sub>2</sub> platelets embedded in the MoDTC/ZDDP tribofilm matrix on the disc surfaces.

The wear scar on disc samples was analyzed using Raman mapping. The maps were taken from an area of 80×30 μm<sup>2</sup> in the center of the wear scar with 2 μm intervals between points both in X (across) and Y (along) directions as shown in Figure 1B where Δ<sub>x</sub>=Δ<sub>y</sub>=2 μm. Thus, the maps consisted of 41×16 individual Raman spectra. The width of the Raman map across the wear scar was selected to be the Hertzian contact width, while the length along the wear scar was much shorter as the distribution of MoS<sub>2</sub> tribofilm in this direction was assumed to be continuous. The distribution of MoS<sub>2</sub> tribofilm is uneven along the wear scar on the sample discs due to the intermittent contact during sliding. For each tribotest, four identified mapping analyses were collected *ex-situ* within different locations on the sample discs in Figure 1C, to average results along the wear track. This analysis area was within the wear tracks, and no edge effects were considered in this paper.

For the Raman characterization, a laser excitation of 488 nm was employed at 1 mW laser power and 20 s exposure time. The radius of laser spots for the 488 nm and the 50x magnification objective is 400 nm, providing the spatial resolution of 800 nm. The MoS<sub>2</sub> distribution at the tribocontacts was characterized by the normalized Raman intensity mapping of the A<sub>1g</sub> symmetry mode (412 cm<sup>-1</sup>). For the numerical study in this work, only the A<sub>1g</sub> peak intensity was taken into consideration because the width of the A<sub>1g</sub> peak is smaller than that of the E<sub>2g</sub>

peak ( $383\text{ cm}^{-1}$ ). According to previous studies, heating effects on the tribofilm can be neglected under the above Raman acquisition parameters.<sup>23</sup>

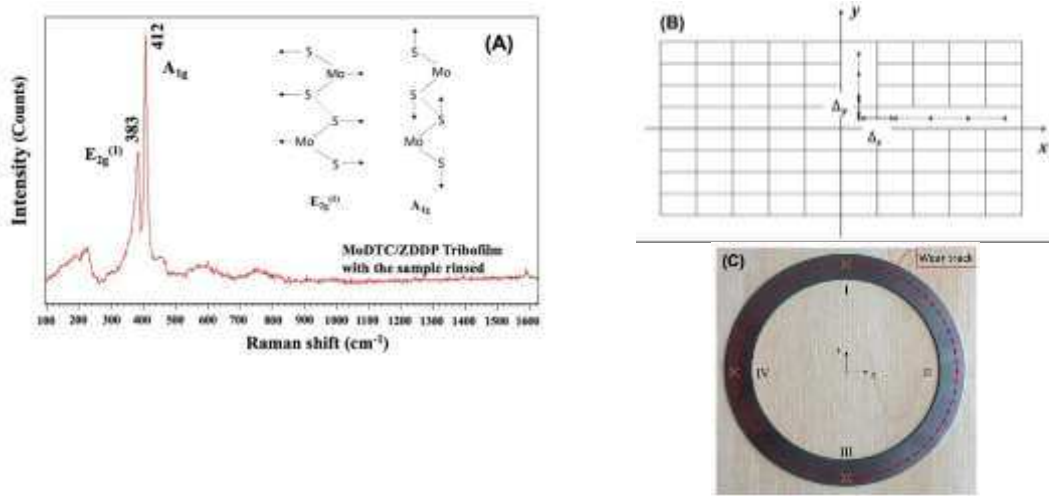


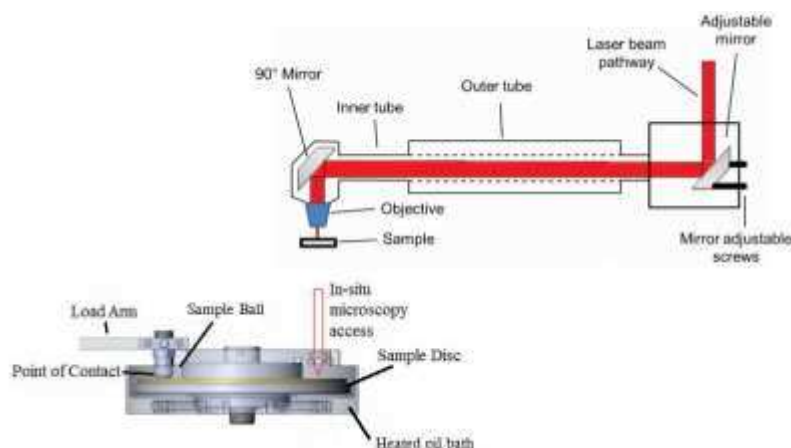
**Figure 1.** (A) Raman spectrum (488 nm excitation) of the MoDTC/ZDDP tribofilm with the illustrations on the motion of atoms for the  $E_{2g}^{(1)}$  and  $A_{1g}$  vibration modes; (B) mesh grids of Raman map calibration; (C) the positions of Raman map calibrations on the disc

**Post-test AFM analyses of the average tribofilm thickness.** During the tribotests, the ball surface is always in contact with the disc, in contrast to the disc surface whose contact is intermittent in any location of the wear track. Hence, the tribofilms on the ball wear scar tend to be thicker and more evenly distributed. Besides, it would be very difficult to measure the tribofilm thickness on the rough counterpart (disc in this case) due to the scale of tribofilm thickness being very close to the surface roughness. Therefore, in order to measure the MoDTC/ZDDP tribofilm thickness, the tribofilm on the ball wear scar was further investigated *ex-situ* by AFM. AFM analyses were taken from an area of  $20\ \mu\text{m} \times 20\ \mu\text{m}$  in the center of the wear scar on the ball samples.

It has been reported that ethylenediaminetetraacetic acid (EDTA) can dissolve the ZDDP tribofilm without damaging the substrate material.<sup>24</sup> At the end of each tribotest, the sample ball was rinsed using heptane, and then microindents were performed within the wear scar on the sample surface. Subsequently, the same region around the microindent was analyzed using AFM following the optical microscope observations twice: (1) before removing the MoDTC/ZDDP tribofilm; (2) after removing the MoDTC/ZDDP tribofilm with 0.5mol/litre EDTA disodium salt in distilled water solution. The above procedure was repeated twice in different regions in the central area of the wear scar for each sample.

**In-situ Raman spectroscopy on MoS<sub>2</sub> tribofilm removal.** To investigate the transient removal of MoS<sub>2</sub> with rubbing time, a methodology based on obtaining the chemistry of tribofilms *in-situ* using Raman Spectroscopy (Figure 2) was developed and used. In this technique, the tests were performed in which the MoDTC/ZDDP tribofilm was first formed for 1h using the base oil containing 1%wt ZDDP and 0.5%wt MoDTC. After that, the

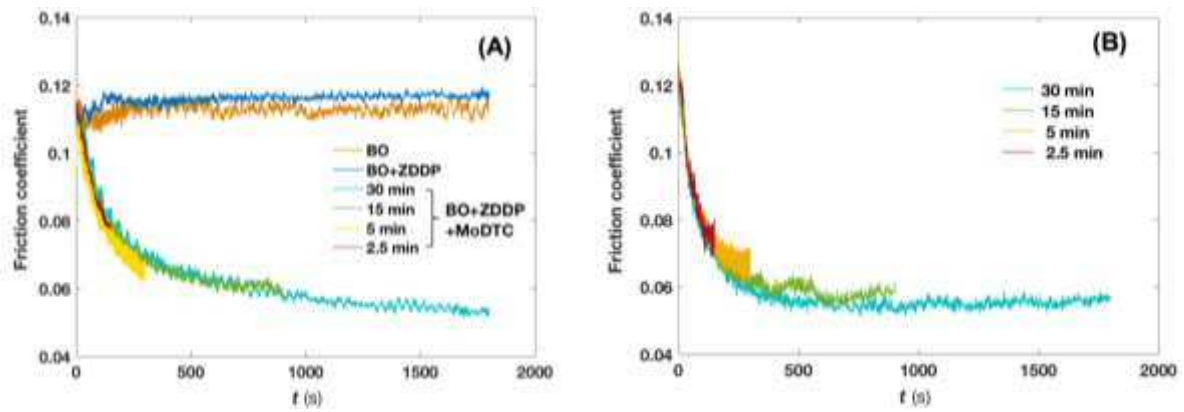
tribometer was halted to drain the initial oil and replace it with a fresh oil containing only 1%wt ZDDP (no MoDTC additive). Care was taken to wipe out the initial oil from the disc surface very gently with a lint-free tissue. After resuming the tribotest with the ZDDP oil, the test was paused periodically to collect *in-situ* Raman spectra from the same point of the disc wear scar. Periodically halting and then restoring the contact between the rubbing surfaces result in a high friction at the beginning of every rerun period due to the running-in process, but have little effect on the removal of MoS<sub>2</sub> tribofilm. *In-situ* Raman spectra were acquired using the flexible sampling arm (in Figure 2) with a laser excitation of 488 nm at 50% laser power and 20 s exposure time. During the entire duration of MoS<sub>2</sub> tribofilm removal tests, the *in-situ* Raman analyses were conducted without removing the lubricant from the sample disc surfaces. The same experimental procedure was conducted at 80 °C and 120 °C. Considering that the temperature difference used in this study is not large, the temperature dependence of the Raman peak intensity can be neglected.



**Figure 2.** Illustration for experimental set-up for *in-situ* Raman spectroscopy<sup>25</sup>

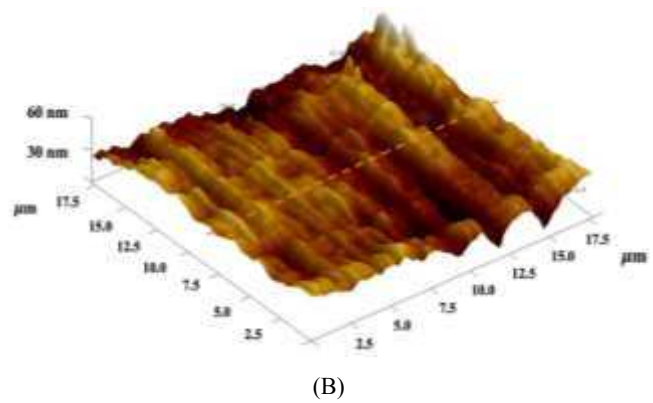
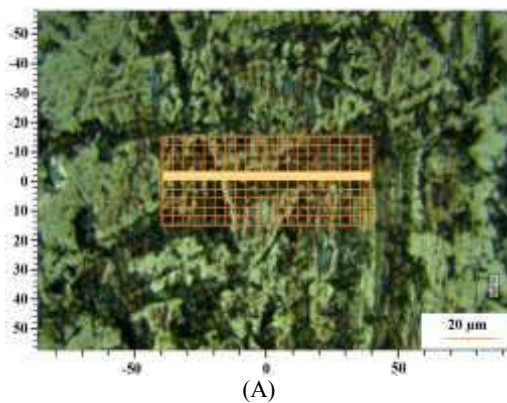
## RAMAN MAPPING CALIBRATIONS

**Ex-situ Raman maps of MoS<sub>2</sub> tribofilm growth.** Figure 3 shows the friction coefficient as a function of time during tests performed at two different temperature conditions. From Figure 3A, it can be seen that the rapid friction drop after a very short induction time was present only when the MoDTC additive in the oil. It could also be seen that the friction coefficient decreases more rapidly by increasing the oil temperature. At both temperatures, the friction coefficient kept the same low values (both between 0.05 and 0.06) after 30 minutes of sliding.



**Figure 3.** Friction coefficient as a function of time for PAO with 0.5%wt MoDTC and 1%wt ZDDP lubricant additives at (A) 80 °C, (B) 120 °C for different test durations (2.5 to 30 minutes), with experimental parameters of 1GPa Hertzian contact pressure and sliding speed of 0.25 m/s

Figure 4A shows the optical micrograph of the disc's wear scar with a MoDTC/ZDDP tribofilm; the rectangular grid indicates the scan area of the *ex-situ* Raman map. Longitudinal roughness patterns are often observed on the wear scar due to running-in and wear, albeit the initial roughness is isotropic. After a short period of rubbing time, the MoS<sub>2</sub> tribofilm is distributed longitudinally along the rubbing track (in all of the figures, the sliding direction is from up to down). Figure 4D shows the Raman intensity profile matching the data obtained by the Raman map in Figure 4C, whereas Figure 4E was obtained from the cross section of the AFM map displayed in Figure 4B. Comparing Figures 4D and 4E, it can be confirmed that the grid point analyses with Raman spectroscopy cover both asperities and valleys, providing a good representation of MoS<sub>2</sub> distribution on the anisotropic surface of the wear scar.



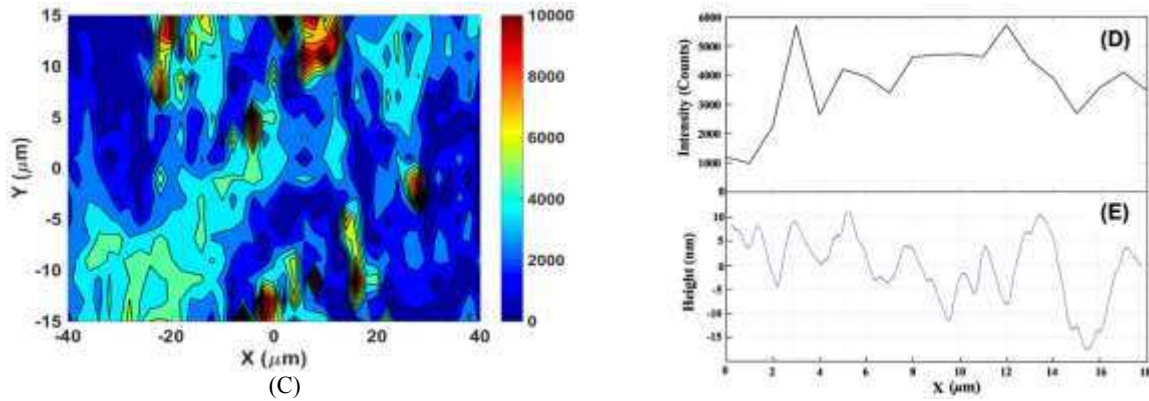


**Figure 4.** Surface characteristics after 15 minutes of rubbing at 120 °C (A) Optical micrograph of the disc's wear scar, (B) 3D AFM image on the disc's wear scar, (C) Raman map of the  $A_{1g}$  peak intensity, (D) Raman Intensity profile (E) Surface topography profile

Figure 5 shows a series of  $80\ \mu\text{m} \times 30\ \mu\text{m}$  Raman map analyses of discs wear scars obtained from tests at different durations at 80 °C and 120 °C. To assess the  $\text{MoS}_2$  tribofilm build-up within the tribocontacts, the same scale bar of  $A_{1g}$  peak intensity is used for each map. The obtained Raman intensity maps evidence that  $\text{MoS}_2$  tribofilm gradually builds up at sliding interfaces with rubbing time. This tribofilm build-up corresponds to a decrease in the friction values obtained at the end of the different time-resolved tests displayed in Figure 3, and displayed at the foot of every Raman map in Figure 5 next to the test duration. At the initial period of rubbing (2.5 minutes), a high intensity of  $A_{1g}$  peak was only observed in isolated regions, and thus the friction coefficient was still high (0.07~0.08 corresponding to Figures 5A and 5I). Rapid friction drops were however observed with further rubbing, together with a much stronger response of the  $A_{1g}$  peak intensity detected in most of the tribocontacted area, indicating that the  $\text{MoS}_2$  tribofilm coverage propagates on the wear scar with rubbing time (Figures. 5B to 5D and 5II to 5IV). We can also see how this evolution and propagation of  $\text{MoS}_2$  tribofilm coverage happens faster at 120 °C. During the steady state, where low friction occurs, high-intensity regions agglomerate and occupy the tribocontact area.

Whether the friction coefficient can be predicted from Raman intensity maps and how the Raman maps can be used to understand the relationship between  $\text{MoS}_2$  distribution and amount and the friction behavior are the principal aspects of tribochemistry to be addressed in this study. The following section will present two models based on the relationship between the friction behavior and the  $\text{MoS}_2$  tribofilm amount and distribution from Raman mapping calibration results.

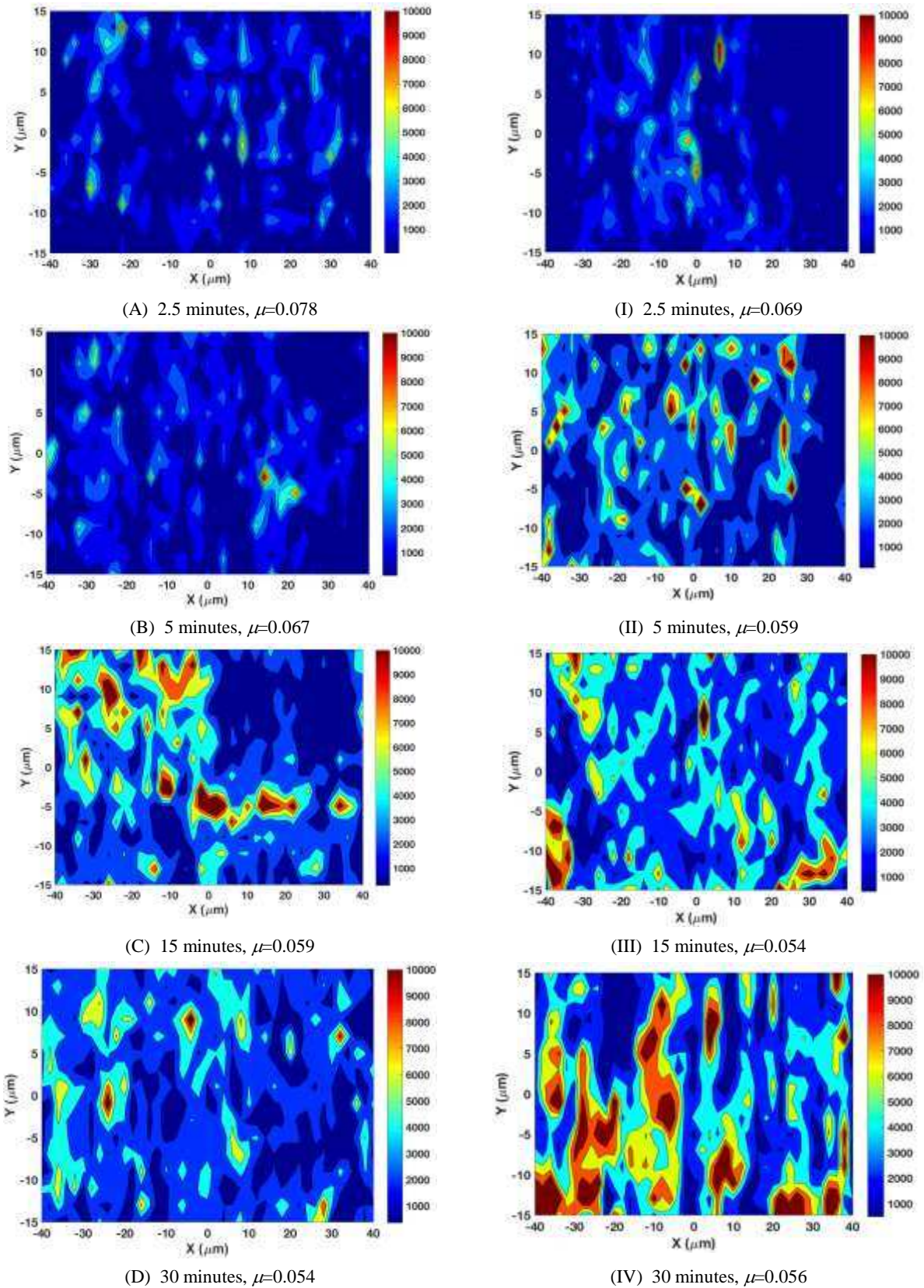


**Figure 5.** *Ex-situ* Raman maps of the  $A_{1g}$  peak intensity at (A-D) 80 °C and (I-IV) 120 °C during different periods of rubbing

**Two models of friction reduction using Raman spectroscopy. Model I:  $MoS_2$  tribofilm coverage**

versus friction coefficient. If  $\alpha$  is defined as the coverage ratio of MoS<sub>2</sub> tribofilm on the contacted area, thus, based on a linear rule-of-mixtures,<sup>26,27</sup> the expression for the friction coefficient can be expressed as

$$\mu = \alpha\mu_{\text{low}} + (1 - \alpha)\mu_{\text{high}} \quad (3)$$

where the high friction coefficient  $\mu_{\text{high}}$  is observed as the initial value of friction coefficient in Figure 6A (0.11 at 80 °C and 0.12 at 120 °C), corresponding to oxides or phosphates-containing tribofilm friction performance as seen in Figure 3A.  $\mu_{\text{low}}$  denotes the low friction coefficient where the contacted areas are covered by sufficient MoS<sub>2</sub> nanosheets. A friction coefficient value of 0.04 was found to be a limiting value in a range of testing conditions<sup>16,25</sup> where only the MoDTC additive was blended in the base oil. The real surface area is less than the nominal contact area. It is also assumed that MoS<sub>2</sub> tribofilms form in the contact at asperities where the appropriate contact conditions occur. As such, there are always some regions where these contact conditions have not been met. Hence, the coverage cannot approach unity, which means  $\alpha < 1$ . Since the friction coefficients have been measured (shown in Figure 3), the corresponding coverages of MoS<sub>2</sub> tribofilm can be directly obtained according to the above equation, as plotted against sliding time in Figure 6A.

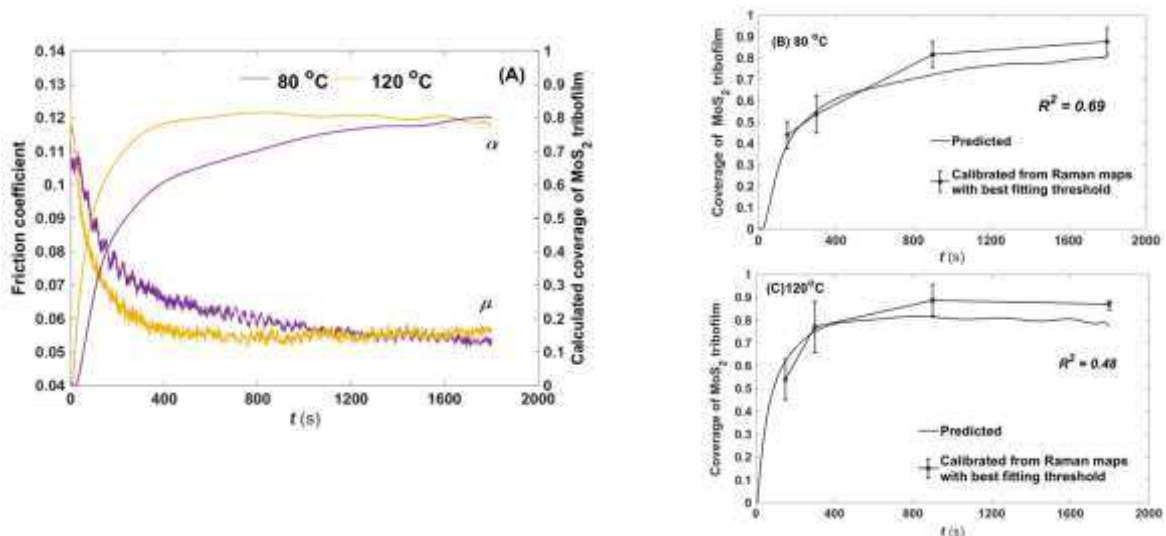


**Figure 6.** (A) Friction coefficient and coverage of MoS<sub>2</sub> tribofilm as various sliding time, (B) Calibrated coverage of MoS<sub>2</sub> tribofilm from Raman maps at 80 °C using Model I, (C) Calibrated coverage of MoS<sub>2</sub> tribofilm from Raman maps at 120 °C using Model I

By setting up a threshold, the Raman intensity map was divided into two areas: low friction areas (with intensity above the threshold) and high friction areas (with intensity below the threshold). The MoS<sub>2</sub> coverage can be determined by the low friction area to the entire area ratio. A range of threshold values were implemented to the Raman intensity maps, and the coverage ratio calibrated from the Raman mapping analyses was then compared to that predicted from the friction coefficient in order to determine best fitting threshold values. The best fitting

results for Model I are shown in Figures 6B and 6C with the threshold values of 1017 counts at 80 °C and 1147 counts at 120 °C. It can be seen that the coverage ratios calibrated from Raman maps are in good agreement with those calculated from friction coefficient values using Eqn. 3 at both temperatures.

*Model II: MoS<sub>2</sub> tribofilm amount versus friction coefficient.* Figure 7 shows the friction coefficient as a function of the integrated intensity of A<sub>1g</sub> peaks obtained from Raman maps. From Figure 7, it can be suggested that the friction drops dramatically as the sum of the intensities, or amount of MoS<sub>2</sub> tribofilm, increases on the wear track. However, friction reduction is ceased when the integrated intensity reaches a plateau. This is consistent with the fact that there is always a limit for low friction coefficient which could be achieved using MoDTC-containing oils.<sup>2</sup> According to this, it is reasonable to introduce the following relationship between the friction coefficient and the intensity of MoS<sub>2</sub> tribofilm in the local tribocontact, illustrated in Figure 8 where two models are compared

$$\mu(i, j) = \begin{cases} \mu_{\text{high}} - \frac{\mu_{\text{high}} - \mu_{\text{low}}}{I_{\text{threshold}}} \times I(i, j), & I(i, j) < I_{\text{threshold}} \\ \mu_{\text{low}}, & I(i, j) \geq I_{\text{threshold}} \end{cases} \quad (4)$$

where  $\mu(i, j)$  and  $I(i, j)$  denote the microscopic friction coefficient and local Raman peak intensity at the spot  $(i, j)$ .

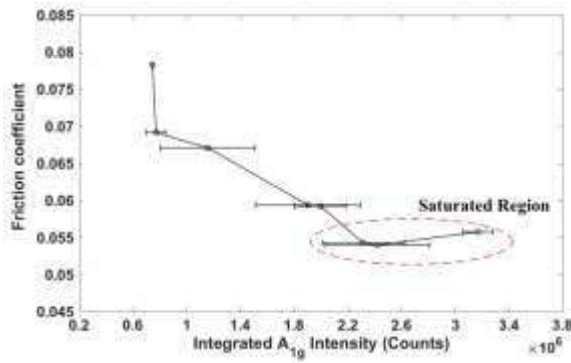


**Figure 7.** Friction coefficients versus the integrated A<sub>1g</sub> peak intensity from the Raman maps

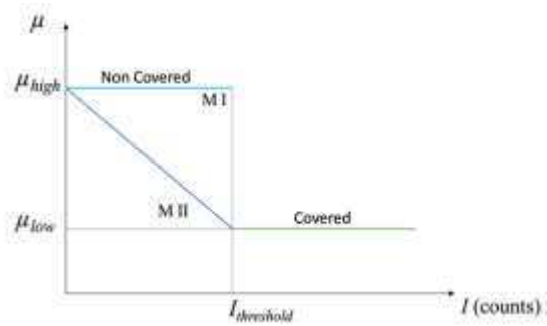


**Figure 8.** The relationship between local A<sub>1g</sub> peak intensity and friction coefficient employed by Model I and II

The microscopic friction coefficient of the tribocontact decreases linearly with an increase in the A<sub>1g</sub> peak intensity until the threshold value is reached, and then friction drop is terminated. Then, the friction coefficient can be determined by averaging the microscopic friction coefficients obtained from Eqn. 4. A specific threshold (2295 counts at 80 °C and 2261 counts at 120 °C) can be found to best fit the curves of the measured friction coefficient using the Model II. Comparisons between the friction coefficient measurements and the calibrations from Raman intensity maps are presented in Figure 9. With the best fit threshold for A<sub>1g</sub> peak intensity, friction coefficients calibrated from the Raman mapping characterization are in accordance with the measured values.

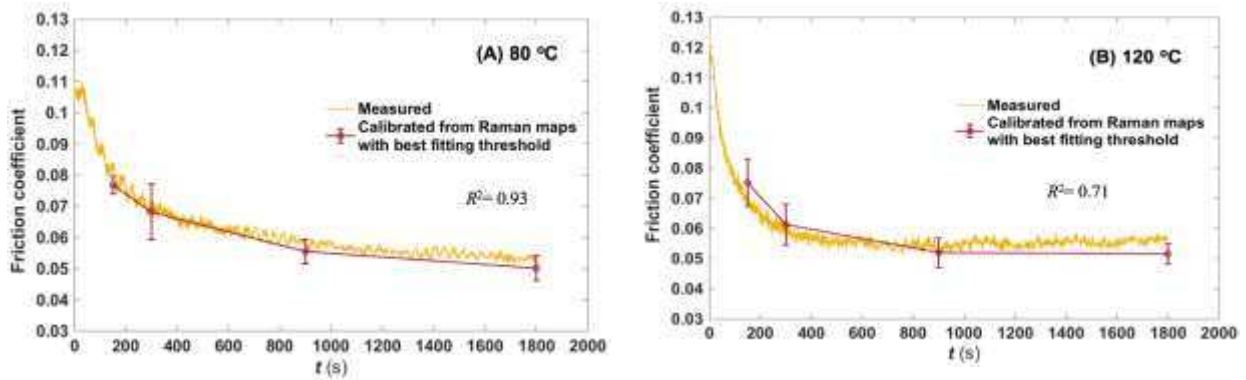


**Figure 9.** Friction coefficient as a function of sliding time with measured values and calibrations from Raman maps by various intensity thresholds at (A) 80 °C, (B) 120 °C

*Model I versus Model II.* In the previous section, two models are presented and suggested as useful tools to link friction drop with the MoS<sub>2</sub> amount/distribution on the wear scar. Model I adopted a binary relation to represent the frictional area covered or non-covered by MoS<sub>2</sub> tribofilm while a linear relationship between the local friction and amount of MoS<sub>2</sub> tribofilm was employed by Model II, as illustrated in Figure 8. The core aspect of the discussion between these two models lies in whether the coverage *or* the amount of MoS<sub>2</sub> determines the friction performance.

By using Model I, an understanding of the link between the MoS<sub>2</sub> tribofilm quantity and distribution and the friction reduction has been proposed. At the tribocontact, low friction is present immediately only when the amount of MoS<sub>2</sub> tribofilm approaches the threshold value, indicating the tribocontacted area is fully covered by the MoS<sub>2</sub> tribofilm. Otherwise, the friction will remain high even if there are some MoS<sub>2</sub> layers formed within the MoDCT/ZDDP tribofilm matrix. In this case, the coverage ratio of MoS<sub>2</sub> on the surface is attributed to the friction drop.

Based on Model II, another explanation to the friction reduction due to the amount and distribution of MoS<sub>2</sub> tribofilm could be obtained. At the tribocontact, friction coefficient will start to reduce once there are some MoS<sub>2</sub> nanosheets formed on the rubbing surface, until the amount of MoS<sub>2</sub> tribofilm reaches what is referred to as a ‘saturated region’. Within this region, the microscopic friction coefficient will remain low even if there is more MoS<sub>2</sub> formed afterwards. This microscopic phenomenon corresponds to the macroscopic friction observation since the friction drop indeed will terminate during sliding.

Table 3 lists the best fitting threshold values obtained from both models under different temperatures, and subsequently the corresponding errors between measured and predicted friction coefficients in the model fit are presented in Table 4. For both models, similar threshold values have been found for the tests run at different temperatures, indicating that the threshold is not dependent on the test temperature. The thresholds obtained by

Model II are higher than those by Model I. It can be seen from Table 4 that the residuals at both test temperatures are larger in Model I than those in Model II. From the perspective of friction prediction accuracy, the better fit ( $R^2$ ) was achieved by using Model II. Although the linear relationship between the Raman intensity and friction coefficient presented with the Model II could be much more complex than Model I, this linear relationship still provides a good fit to the friction measurement. In Figure 7, the integrated  $A_{1g}$  peak intensity reaches around  $1.8 \times 10^6$  counts (corresponding to the average value of 2743 counts) before the friction drop reaches a plateau. This estimated value is in close agreement with the intensity threshold (2295 counts) in Model II.

**Table 3** Best fitting  $A_{1g}$  peak Intensity threshold values in counts

Threshold (counts)	Model I	Model II
80 °C	1017	2295
120 °C	1147	2261

**Table 4** The sum of squares error (SSE)

SSE	Model I	Model II
80 °C	$1.02 \times 10^{-4}$	$2.48 \times 10^{-5}$
120 °C	$1.23 \times 10^{-4}$	$5.30 \times 10^{-5}$
Goodness of fit	51.87 %	83.37%

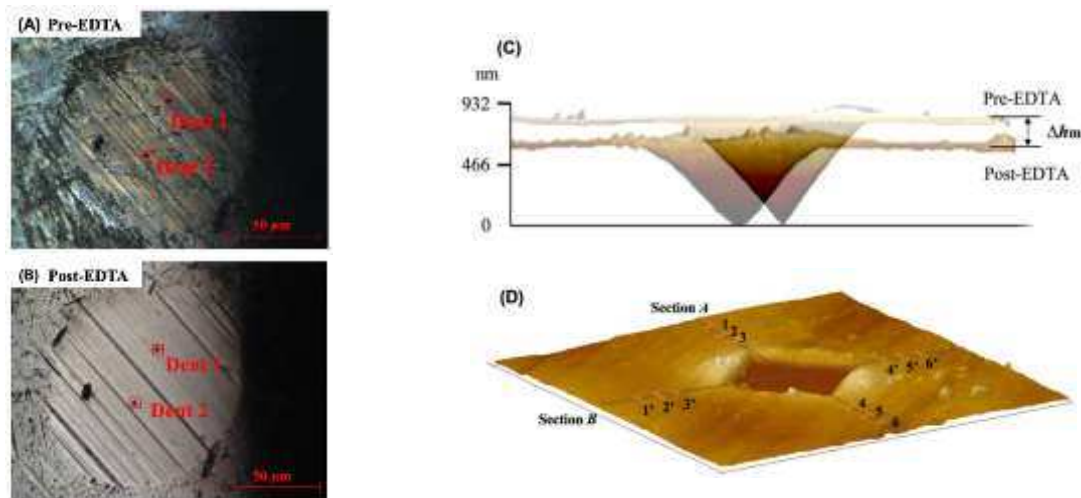
Therefore, a new insight into how the  $MoS_2$  tribofilm build-up is attributed to the friction reduction can be acquired by comparison of the two proposed models. The coverage ratio, as well as the amount of  $MoS_2$ , will have an influence on the friction behavior. In the first stage, the friction reduction is mainly due to the amount of  $MoS_2$  growth. The friction drop begins immediately at the microscopic tribocontact when the  $MoS_2$  nanosheets are formed on the rubbing surface. But once the quantity of  $MoS_2$  reaches a saturated value, the tribocontacted area is fully covered by the  $MoS_2$  tribofilm, and subsequently, the friction reduction will cease within this area. During this stage, the final friction coefficient value mainly depends on the coverage of  $MoS_2$  on the surface.

## EVOLUTION OF THE TRIBOFILM THICKNESS

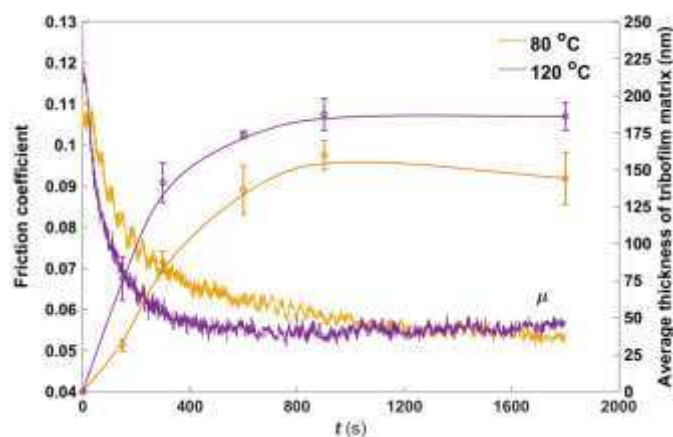
The optical micrographs of the balls wear scars, as shown in Figures 10A and 10B, clearly demonstrate that the MoDTC/ZDDP tribofilm has been entirely removed from the surface by EDTA treatment. In this section, pre-EDTA is corresponding to surfaces before removing the tribofilm while post-EDTA corresponds to surfaces after EDTA treatment. As shown in Figure 10C, the three-dimensional surface topographies generated by pre-EDTA and post-EDTA AFM were set upon the same baseline under the same scale, and then the difference in height can be obtained between them, representing the average MoDTC/ZDDP tribofilm thickness. One of the complexities of the  $MoS_2$  system in a tribofilm is that the  $MoS_2$  tribofilm is not continuous.

To minimize the effect of plastic flow due to microindentations, two-dimensional sections along the diagonal direction of the microindentation were taken and a series of heights from the surface to the bottom of the microindentation were measured for each AFM analysis, as shown in Figure 10D. Finally, the average tribofilm

thickness was acquired when using the average height of pre-EDTA treatment compared to that of post-EDTA treatment ( $\Delta h = H_0 - H_1$ ). With this method, the indenter penetrates the entire depth of the tribofilm reaching the substrate material.



**Figure 10.** Optical micrographs (A, B) on the sample balls wear scar at 80 °C after 15 minutes of rubbing; (C) 3D AFM images on pre-EDTA and post-EDTA surface topographies on the sample ball wear scar at 80 °C after 15 minutes of rubbing time; (D) Illustration on the AFM analysis



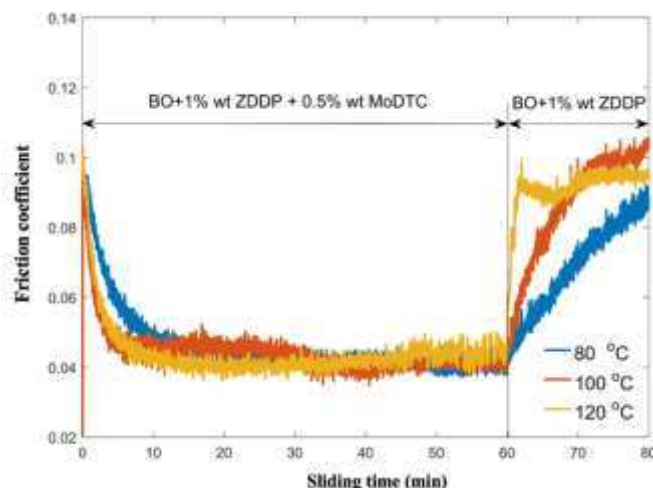
**Figure 11.** MoDTC/ZDDP tribofilm thickness evolution as a function of sliding time

Figure 11 shows the evolution of the average MoDTC/ZDDP tribofilm thickness as a function of sliding time at 80 °C and 120 °C tribological tests, obtained after different rubbing durations. It can be seen that, at both temperatures, the MoDTC/ZDDP tribofilm thickness levels out to a steady state value in the range from 150 to 200 nm after a rubbing period. It can also be seen that the formation rate for the tribofilm thickness at 120 °C is higher than that at 80 °C. These trends, as well as the range of film thickness values, are in close agreement with the results from previous experiments.<sup>28</sup>

### **IN-SITU TRIBOFILM REMOVAL**

In Figure 12, the friction coefficient curves obtained from MoS<sub>2</sub> tribofilm removal tests are shown. In these

tests, the MoDTC/ZDDP tribofilm was first formed on the rubbing surface before the oil was replaced by the lubricant free from the MoDTC additive but containing ZDDP. With no MoDTC additive in the lubricant, the low friction coefficient obtained with the MoDTC/ZDDP tribofilm starts immediately to increase until levelling out at a high level. Figure 12 shows that the test temperature significantly affects the rate by which the low friction increases.



**Figure 12.** Friction coefficient as a function of time at 80 °C, 100 °C and 120 °C, with changing the lubricants from PAO with 1%wt ZDDP and 0.5%wt MoDTC lubricant additives to PAO with 1%wt ZDDP after 60 minutes of rubbing time, with experimental parameters of 1GPa Hertzian contact pressure and sliding speed of 0.25 m/s

Raman analyses, as shown in Figures 13A and 13B, demonstrate the removal behavior of MoS<sub>2</sub> nanocrystal flakes in the MoDTC/ZDDP tribofilm matrix at different temperatures. Significant reductions were observed in the spectra (the E<sub>12g</sub> and A<sub>1g</sub> peaks around the Raman shifts of 383 and 412 cm<sup>-1</sup>) as removal progressed. The other peaks at 850 cm<sup>-1</sup>, 1071 cm<sup>-1</sup>, 1301 cm<sup>-1</sup>, 1444 cm<sup>-1</sup> observed in Figures 13A and 13B belong to the base oil, and no significant changes were observed in these peaks with rubbing time. A few MoS<sub>2</sub> layers seemed to remain on the MoDTC/ZDDP tribofilm surface even after a 20-minute removal test. This suggests that some MoS<sub>2</sub> is embedded in the MoDTC/ZDDP tribofilm matrix instead of being on top of that, and thus, the tribofilm matrix can effectively protect the MoS<sub>2</sub> nano flakes from being abraded. Alternatively, it could indicate that there is some MoS<sub>2</sub> tribofilm remaining on the wear scar, rather than being completely removed. However, none of these remaining MoS<sub>2</sub> sheets could maintain the low friction behavior.

To reduce the errors from positioning and measurement resolution of *in-situ* Raman analyses, a small Raman map was undertaken within the area of 3×3 μm<sup>2</sup> and 9 single Raman spectra were obtained at this area. Then, the average normalized intensity of the A<sub>1g</sub> peak was calculated from them, and plotted in Figure 13C, as a function of removal time. It can be seen that the Raman intensities of MoS<sub>2</sub> species exponentially decay as a function of removal time. During the end period of removal tests at both temperatures, the intensities of the A<sub>1g</sub> peak

maintained at a nonzero level and similar values were observed under different temperature conditions.

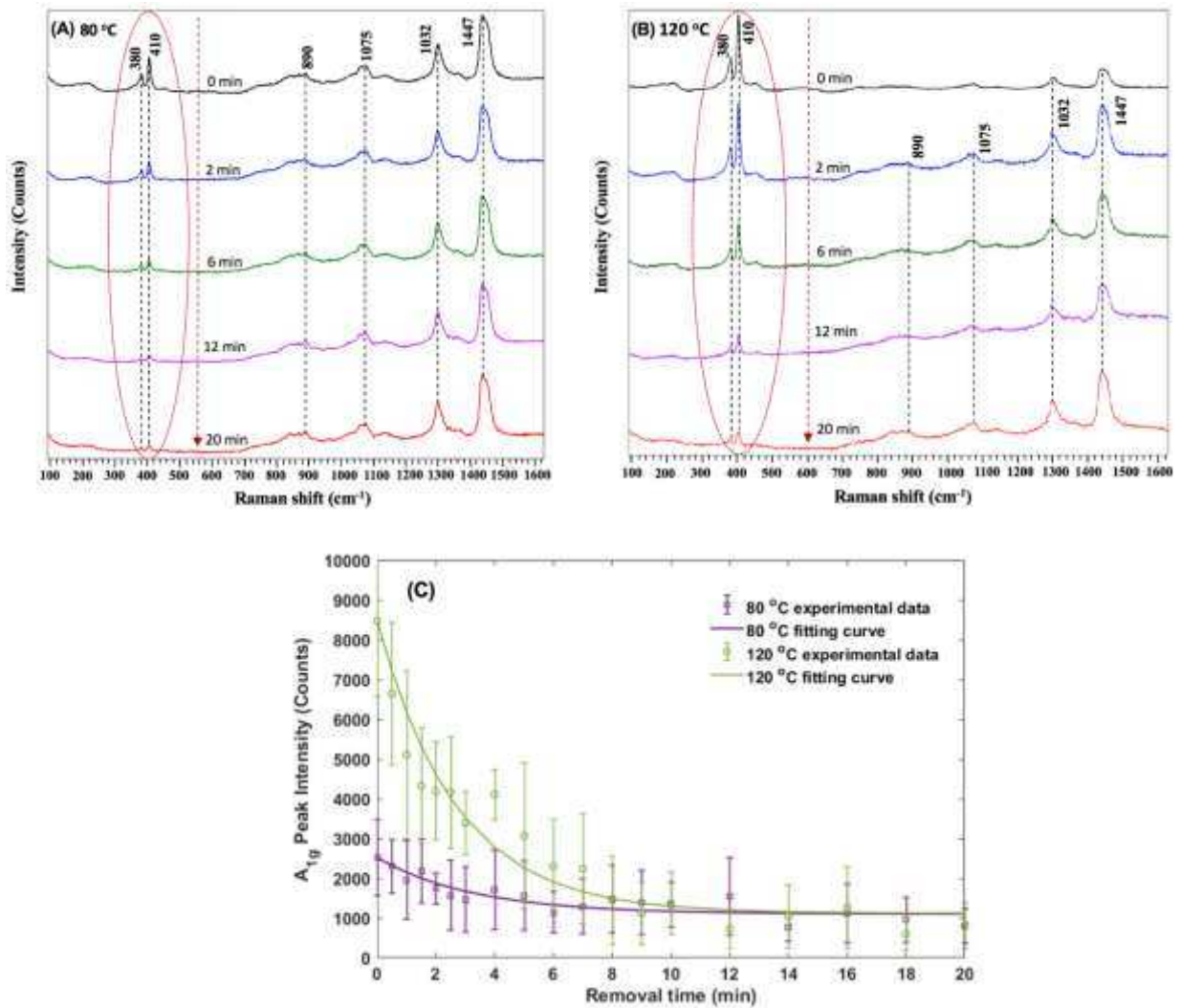


**Figure 13.** (A) Variations of Raman spectra as a function of removal time at 80 °C, (B) Variations of Raman spectra as a function of removal time at 120 °C, (C) Fitting curves to the A<sub>1g</sub> peak intensity as a function of removal time at 80 °C and 120 °C

The fitting curve for the normalized intensity of the A<sub>1g</sub> peak removal can be expressed by the following equation

$$I = I_0 - C_1(1 - e^{-C_2 t}) \quad (5)$$

where the constant  $C_2$  denotes the removal rate of MoS<sub>2</sub> species with the values of 0.0056 (s<sup>-1</sup>) at 80 °C and 0.0065 (s<sup>-1</sup>) at 120 °C, respectively. The starting value of Raman intensity is different at 80 °C and 120 °C, but the decay rate constants are similar. Compared to the results of ZDDP tribofilm removal exponential factor, these values are considerably higher than those obtained by Ghanbarzadeh et al. of 0.0004~0.0006799.<sup>29</sup> This strongly suggests that compared to anti-wear ZDDP tribofilm, the MoS<sub>2</sub> nanocrystal sheets are much easier to be removed from the tribocontact, especially for those lying on top of the MoDTC/ZDDP tribofilm.

## MoS<sub>2</sub> TRIBOFILM EVOLUTION: AMOUNT AND COVERAGE

From this work, the mechanism of how the MoS<sub>2</sub> tribofilm builds up in the MoDTC/ZDDP tribofilm matrix is presented below and illustrated in Figure 14. At the initial rubbing period, only a few areas are covered by MoS<sub>2</sub> nanocrystal flakes, the MoDTC/ZDDP tribofilm matrix is very thin and amorphous-like structures of MoS<sub>2</sub> are dispersed inside. The friction is relatively high in this stage. As the counterparts continue to slide, more and more areas on the wear scar cover by the MoS<sub>2</sub> tribofilm, and layer-lattice structure of MoS<sub>2</sub> forms within the thicker MoDTC/ZDDP tribofilm matrix. Both of these lead to a rapid friction reduction. At this stage, the MoS<sub>2</sub> tribofilm formation rate is much larger than the removal rate in the macroscale.

The structural changes of MoS<sub>2</sub> tribofilm can be observed using TEM analyses.<sup>19</sup> Since the orientation of the MoS<sub>2</sub> crystal growth is along the sliding direction, the change in the MoS<sub>2</sub> structure could be due to the rubbing between the contacted asperities. The friction drop will reach a plateau when the MoS<sub>2</sub> tribofilm coverage reaches a ‘saturated value’. During this period, the chemical balance has been approached, indicating that the tribofilm formation rate is equal to the removal rate in the macroscale.

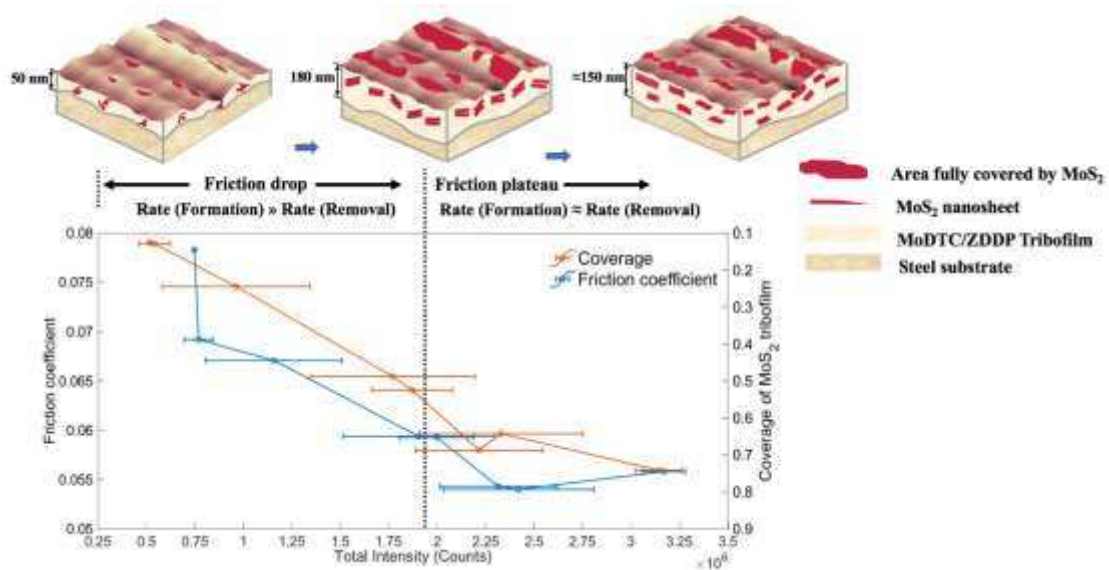


**Figure 14.** Schematic diagram of the MoDTC-derived tribofilm evolution

## CONCLUSIONS

In this study, experimental and analytical models based on Raman spectroscopy and AFM have been proposed toward quantitatively understanding the link between the friction performance and the MoS<sub>2</sub> tribofilm build-up in the boundary lubrication regime. The framework set out in this study can also be extended to analyze the MoS<sub>2</sub> tribofilm formation and removal for the DLC/steel and DLC/DLC rubbing pairs in the future work.

Key conclusions, listed below, provide the basis for the development of a semi-deterministic numerical model capable of predicting friction coefficient based on MoS<sub>2</sub> tribofilm distribution; the subject of a following-up paper.

- (1) *Ex-situ* Raman intensity map calibrations were carried out on the wear track during different sliding periods. With the implementation of two specific calibration methodologies, the  $A_{1g}$  peak intensity threshold for low friction area was obtained, and then employed to predict the  $MoS_2$  tribofilm coverage growth and subsequently the friction reduction during rubbing. A better prediction accuracy was achieved with the Model II, which is based on the assumption of a linear relationship between the friction coefficient and the local amount of  $MoS_2$  tribofilm on the wear scar.
- (2) By post-test AFM analysis, the average MoDTC/ZDDP tribofilm thickness on the wear scar was measured. After a rapid increase, the average thickness of the MoDTC/ZDDP tribofilm matrix levels out to a steady state value in the range from 150 to 200 nm.
- (3) *In-situ* Raman spectrum analyses detected the  $MoS_2$  tribofilm removal on the MoDTC/ZDDP tribofilm surfaces after removing the MoDTC additive from the lubricant. An understanding of removal mechanism of  $MoS_2$  films was obtained. The removal of  $MoS_2$  tribofilm is much easier compared to the removal of a robust ZDDP tribofilm, causing the loss of effectiveness of  $MoS_2$  tribofilms on providing low friction when MoDTC is not present.
- (4) A new insight into the link between the  $MoS_2$  tribofilm build-up and the friction performance has been developed. The formation of a  $MoS_2$  tribofilm at local tribocontacts immediately results in the microscopic friction reduction, but the drop is terminated once the amount of  $MoS_2$  reaches what is referred to as a 'saturated value'. The balance is reached between the  $MoS_2$  formation and removal in the 'saturated region'.

## **AUTHOR INFORMATION**

### **Corresponding Authors**

\*Email: a.morina@leeds.ac.uk; d.l.xu@leeds.ac.uk

### **ORCID**

Dichu Xu: 0000-0002-3236-6715

Cayetano Espejo: 000-0001-7139-3807

Jiugen Wang: 0000-0001-8720-1005

Anne Neville: 0000-0002-6479-1871

Ardian Morina: 0000-0001-8868-2664

### **Notes**

The authors declare no competing financial interest.

## **ACKNOWLEDGMENTS**

The authors are grateful for the financial support of the National Natural Science Foundation of China (Grant No.51375436), National Hi-tech Research and Development Program of China (863 Program, Grant No. 2015AA043002), Key Project of Science and Technology of Zhejiang Province (Grant No. 2017C01047) and China Scholarship Council (CSC) for sponsorship of this research.

## **REFERENCES**

- (1) Holmberg, K.; Andersson, P.; Erdemir, A. Global energy consumption due to friction in passenger cars. *Tribol. Int.* **2012**, *47*(0), 221-234.
- (2) Morina, A.; Neville, A. Tribofilms: aspects of formation, stability and removal. *J. Phys. D: Appl. Phys.* **2007**, *40*(18), 5476-5487.

- (3) Spikes, H. Friction modifier additives. *Tribol. Lett.* **2015**, *60*(1): 5.
- (4) Bosman, R.; Schipper, D. J. Mild wear prediction of boundary-lubricated contacts. *Tribol. Lett.* **2011**, *42*(2), 169-178.
- (5) Akchurin, A.; Bosman, R. A Deterministic Stress-Activated Model for Tribo-Film Growth and Wear Simulation. *Tribol. Lett.* **2017**, *65*(2), 59.
- (6) Piras, F.M.; Rossi, A.; Spencer, N.D. Growth of tribological films: in situ characterization based on attenuated total reflection infrared spectroscopy. *Langmuir* **2002**, *18*(17), 6606-6613.
- (7) Ewen, J.P.; Gattinoni, C.; Morgan, N.; Spikes, H.A.; Dini, D. Nonequilibrium molecular dynamics simulations of organic friction modifiers adsorbed on iron oxide surfaces. *Langmuir* **2016**, *32*(18), 4450-4463.
- (8) Grossiord, C. K. J. M. T. C. K.; Varlot, K.; Martin, J. M.; Le Mogne, T.; Esnouf, C.; Inoue, K. MoS<sub>2</sub> single sheet lubrication by molybdenum dithiocarbamate. *Tribol. Int.* **1998**, *31*(12), 737-743.
- (9) Onodera, T.; Morita, Y.; Suzuki, A.; Koyama, M.; Tsuboi, H.; Hatakeyama, N.; Endou, A.; Takaba, H.; Kubo, M.; Dassenoy, F.; Minfray, C. A computational chemistry study on friction of h-MoS<sub>2</sub>. Part I. Mechanism of single sheet lubrication. *J. Phys. Chem. B* **2009**, *113*(52), 16526-16536.
- (10) Gosvami, N. N.; Bares, J. A.; Mangolini, F.; Konicek, A. R.; Yablon, D. G.; Carpick, R. W. Mechanisms of antiwear tribofilm growth revealed in situ by single-asperity sliding contacts. *Science* **2015**, *348*(6230), 102-106.
- (11) Zhang, J.; Spikes, H. On the mechanism of ZDDP antiwear film formation. *Tribol. Lett.* **2016**, *63*(2), 1-15.
- (12) He, X.; Kim, S.H. Mechanochemistry of physisorbed molecules at tribological interfaces: molecular structure dependence of tribochemical polymerization. *Langmuir* **2017**, *33*(11), 2717-2724.
- (13) Tysoe, W. On Stress-Induced Tribochemical Reaction Rates. *Tribol. Lett.* **2017**, *65*(2), 48.
- (14) Dallavalle, M.; Sändig, N.; Zerbetto, F. Stability, dynamics, and lubrication of MoS<sub>2</sub> platelets and nanotubes. *Langmuir* **2012**, *28*(19), 7393-7400.
- (15) Morina, A.; Neville, A.; Priest, M.; Green, J.H. ZDDP and MoDTC interactions and their effect on tribological performance—tribofilm characteristics and its evolution. *Tribol. Lett.* **2006**, *24*(3), 243-256.
- (16) de Barros' Bouchet, M. I.; Martin, J. M.; Le-Mogne, T.; Vacher, B. Boundary lubrication mechanisms of carbon coatings by MoDTC and ZDDP additives. *Tribol. Int.* **2005**, *38*(3), 257-264.
- (17) Graham, J.; Spikes, H.; Jensen, R. The friction reducing properties of molybdenum dialkyldithiocarbamate additives: Part II-Durability of friction reducing capability. *Tribol. Trans.* **2001**, *44*(4), 637-647.
- (18) Miklozic, K.T.; Graham, J.; Spikes, H. Chemical and physical analysis of reaction films formed by molybdenum dialkyl-dithiocarbamate friction modifier additive using Raman and atomic force microscopy. *Tribol. Lett.* **2001**, *11*(2), 71-81.
- (19) Rai, Y.; Neville, A.; Morina, A. Transient processes of MoS<sub>2</sub> tribofilm formation under boundary lubrication. *Lubr. Sci.* **2016**, *28*(7), 449-471.
- (20) Khaemba, D.N.; Neville, A.; Morina, A. New insights on the decomposition mechanism of Molybdenum DialkyldiThioCarbamate (MoDTC): a Raman spectroscopic study. *RSC Adv.* **2016**, *6*(45), 38637-38646.
- (21) Hamrock, B.J.; Dowson, D. Isothermal elastohydrodynamic lubrication of point contacts: part III—fully flooded results. *J. Lubr. Technol.* **1977**, *99*(2), 264-275.
- (22) Greaves, M. Pressure viscosity coefficients and traction properties of synthetic lubricants for wind turbine gear systems. *Lubr. Sci.* **2012**, *24*(2), 75-83.
- (23) Khaemba, D. N.; Neville, A.; Morina, A. A methodology for Raman characterisation of MoDTC tribofilms and its application in investigating the influence of surface chemistry on friction performance of MoDTC lubricants. *Tribol. Lett.* **2015**, *59*(3), 38.
- (24) Rydel, J.J.; Pagkalis, K.; Kadiric, A.; Rivera-Díaz-del-Castillo, P.E.J. The correlation between ZDDP tribofilm morphology and the microstructure of steel. *Tribol. Int.* **2016**, *113*, 13-25.
- (25) Rai, Y. In-situ Interface Chemical Characterisation of a Boundary Lubricated Contact. Doctoral dissertation, University of Leeds, **2015**.
- (26) Bowden, F. P.; Tabor, D. *The friction and lubrication of solids. Vol. 1 & Vol. 2.* Oxford University Press, **1954, 1964**.
- (27) Blanchet, T.A.; Sawyer, W.G.; Differential application of wear models to fractional thin films. *Wear* **2001**, *251*(1-12), 1003-1008.
- (28) Naveira-Suarez, A.; Tomala, A.; Grahn, M.; Zaccheddu, M.; Pasaribu, R.; Larsson, R. The influence of base oil polarity and slide-roll ratio on additive-derived reaction layer formation. *P. I. Mech. Eng. J: J. Eng. Tribol.* **2011**, *225*(7), 565-576.
- (29) Ghanbarzadeh, A.; Parsaeian, P.; Morina, A.; Wilson, M.C.; van Eijk, M.C.; Nedelcu, I.; Dowson, D.; Neville, A. A semi-deterministic wear model considering the effect of zinc dialkyl dithiophosphate tribofilm. *Tribol. Lett.* **2016**, *61*(1), 12.5

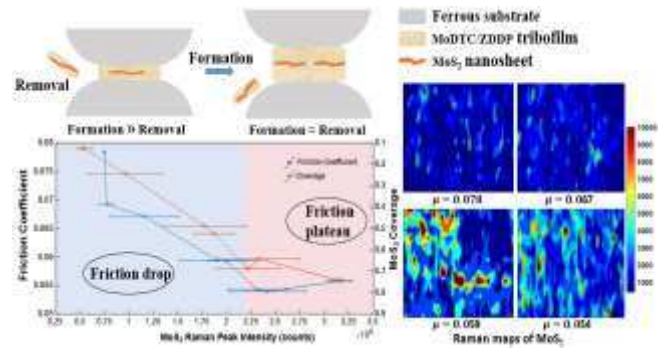


Table of Contents Graphic